TITLE PAGE

Title: Improving Inertial Navigation System Alignment using a Proportional-Integral Left-Invariant Extended Kalman Filter: A Robust Approach Against Inertial Sensors Errors

Running title: Robust INS Alignment with PI-LIEKF

Authors information:

❖ Mohammad Javad Rajabi

Affiliation: Electrical and Computer Faculty, Malek Ashtar University of Technology, Tehran, Iran

E-mail: mjrajabi@mut.ac.ir

❖ S.M.M. Dehghan*

Affiliation: Electrical and Computer Faculty, Malek Ashtar University of Technology, Tehran, Iran

E-mail: smmd@mut.ac.ir

ORCID: https://www.orcid.org/0000-0002-3835-0212

❖ S.Mohammad-Hosseini

Affiliation: Electrical and Computer Faculty, Malek Ashtar University of Technology, Tehran, Iran

E-mail: smhoseini@mut-es.ac.ir

***Corresponding author:**

E-mail: smmd@mut.ac.ir

Telephone: +982122986292

Mobile: +989126442731

Fax: +989126442731

Postal Address: Electrical and Computer Faculty, Malek Ashtar University of Technology, Tehran, P.O. Box 15875-1774, Iran.

Improving Inertial Navigation System Alignment using a Proportional-Integral Left-Invariant Extended Kalman Filter: A Robust Approach Against Inertial Sensors Errors

Mohammad Javad Rajabi[1], S.M.M. Dehghan[2], S. Mohammad-Hosseini[3]

[1,2,3] Electrical and Computer Faculty, Malek Ashtar University of Technology, Tehran, Iran

Abstract

Alignment is a critical pre-processing step before initiating inertial navigation operations. The extended Kalman filter (EKF), commonly employed for aligning strap-down inertial navigation systems (SINS), faces challenges due to linearization limitations. In response to some of these challenges, the invariant extended Kalman filter (IEKF) was developed. A key requirement for utilizing IEKF is that the system dynamics must exhibit a group affine property. However, considering inertial measurement unit (IMU) errors as state variables violates this condition. This paper introduces an improved version of IEKF, named the proportional-integral invariant Extended Kalman Filter (PI-IEKF). This approach initially ignores IMU bias and drift to preserve the group affine property. To compensate for these uncertainties, the Kalman filter's innovation term is reformulated into a proportional-integral (PI) structure. The PI gains are tuned based on Lyapunov stability criteria by solving a Linear Matrix Inequality (LMI). The PI-IEKF not only addresses the uncertainties but also enhances alignment accuracy. The proposed approach was evaluated through simulations and field tests. Simulations addressed the nonlinear alignment problem in marine environment with typical wave disturbances, while field tests used an open-source dataset from vehicle-mounted sensors. Comparative results with conventional IEKF demonstrated significant improvements in convergence speed and robustness.

Keywords

Inertial Navigation System, Initial Alignment, Robust Filtering, Invariant Extended Kalman Filter, Proportional-Integral Innovation

1. Introduction

The inertial navigation system (INS) offers advantages, making it the primary choice for determining position, velocity, and attitude [1]. INS relies on a dead-reckoning navigation method to calculate these variables, necessitating accurate values for position, velocity, and attitude at the beginning of navigation. It is clear that even small errors in these values, especially when navigation aid data is unavailable or disrupted, can lead to significant inaccuracies over time. Thus, the accuracy of initial values greatly influences navigation accuracy. Typically, the initial position and velocity are easily determined using external sources like the Global Positioning System (GPS). However, determining the initial attitude, known as alignment, continues to be a key challenge. The performance of the alignment process is primarily evaluated based on two criteria: accuracy and time [2]. Given the significance of alignment, this topic has been extensively researched. According to the author's knowledge and a general overview, the existing methods for aligning a SINS in the literature are classified into three types: two-stage alignment, nonlinear alignment, and optimization-based alignment (OBA) methods. The most common SINS alignment method is the two-stage approach, which involves two consecutive steps [3]. In the first step, called coarse alignment, a rough but suitable estimate of the initial attitude is provided. The second step, called fine alignment, enhances accuracy by employing a linear model and utilizing optimal estimation techniques, such as the Kalman filter. However, the main drawback of two-stage alignment is its reliance on the performance of the first step and its vulnerability to disturbances and maneuvers of the carrier. In contrast, the nonlinear method aims to eliminate the coarse alignment by using

models and nonlinear filters, thereby reducing the overall alignment time [4]. Research in nonlinear alignment frequently focuses on developing appropriate error models [4, 5], implementing nonlinear filters [6-10], or combining both. OBA also employs attitude matrix decomposition and optimal solution of the Wahba problem to achieve alignment amid disturbances or carrier maneuvers [11]. This method offers advantages such as eliminating the need for error model extraction, as well as improved convergence speed, accuracy, and robustness [12, 13]. However, OBA has limitations, including not providing covariance information [14] and slow convergence under low dynamic conditions [15]. The problem explored in this paper is the alignment of SINS at sea. Given the non-linear nature of this problem, employing a non-linear alignment method is considered suitable. The nonlinear alignment method requires both a nonlinear model and a nonlinear filtering technique. Typically, nonlinear versions of the Kalman filter, particularly the Extended Kalman filter, are employed. The EKF has demonstrated effectiveness across various engineering applications. However, for systems with strong nonlinearities, it can produce unreliable or divergent estimates [16, 17]. Other challenges associated with the EKF include a lack of guaranteed optimality, global convergence issues [18, 19], and consistency problems [20, 21]. The IEKF is a novel adaptation of the EKF, developed to address some of its limitations and improve its performance. This filter is based on the symmetry-preserving observer theory [22]. Unlike the standard Kalman filter, which operates in Euclidean space, the IEKF performs the estimation on the manifold by considering the invariance of the estimation error under the action of the Lie group as the system's symmetry [23]. Reference [23] demonstrates that the IEKF is a locally asymptotically convergent observer for a specific class of systems, namely those that establish the group affine property. When the state lies on a Lie group and the system exhibits this property, the invariant error of the estimate evolves according to an autonomous differential equation, whose linearization is independent of the estimated states. This reduces linearization

error, leading to improved convergence and accuracy. Additionally, it overcomes many of the limitations associated with the Jacobian-based linearization used in the EKF [24]. Many navigation-related problems, such as attitude estimation and alignment, can be addressed using the IEKF framework. In [25], the error state model and invariant measurements are provided for SINS/GNSS integration in the inertial frame. In [26], IEKF has been applied for SINS initial alignment under large azimuth error. The error state model and invariant measurements have been used in various applications, including SINS alignment using the standard Kalman filter [27], rotational INS alignment [28, 29], and SINS transfer alignment [30]. Despite the many advantages of the IEKF, its main challenge lies in fulfilling the group affine property by the system dynamics [23]. This condition is often violated in inertial navigation for two main reasons. The first reason is the strong coupling between navigation variables, which can be addressed by modifying the navigation mechanization [31]. The second reason involves treating the bias and drift errors of inertial sensors as state variables. To handle this, an imperfect IEKF has been employed [32, 33], where the IEKF estimates attitude, velocity, and position, while a conventional EKF is used to estimate sensor errors. Despite the better performance of the imperfect IEKF compared to the EKF and its ability to retain the main advantages of the IEKF, this method does not fully utilize all the advantages of the IEKF [33]. In this paper, a robust method is introduced to address uncertainties arising from the drift and bias of inertial sensors. Unlike conventional approaches that model and estimate these errors as state variables, the proposed method directly mitigates their effects through enhanced robustness against disturbances and uncertainties. The PI filter is the approach adopted for this purpose. Drawing inspiration from the PI controller technique, this method utilizes an integral feedback loop in addition to the proportional feedback loop typically used in conventional methods. This approach not only enhances the robustness of the estimation against the uncertainties but also improves the accuracy of the estimation. The primary contributions of

this study can be summarized in two main aspects: the first is the development of an enhanced version of the IEKF, which overcomes a significant limitation in using it. By disregarding the bias and drift of inertial sensors, this method satisfies the group affine property, thereby enabling the application of the IEKF. Furthermore, a proportional-integral innovation term is employed to address these uncertainties. The second is the application of this improved filter to the alignment of SINS. The structure of this paper is as follows: Section 2 states the problem and assumptions. The theoretical principles of the IEKF are explained in Section 3. Section 4 introduces the proposed method. In Section 5, the navigation variables in the inertial frame are embedded as a matrix Lie group. It is also proved that the error model is state-independent, and a suitable dynamic model for the invariant error and invariant measurements is presented. The performance of the PI-IEKF in SINS alignment is evaluated in Section 6, using simulated data from a marine environment and experimental data. Finally, the last section discusses the results and presents the conclusions.

2. Problem Statement and Assumptions

The problem addressed in this paper is the initial alignment of a SINS. Accurate alignment is essential, since even small initial attitude errors can lead to significant navigation drift, especially when external aiding signals are unavailable. A widely used method for alignment is the EKF; however, the EKF suffers from problems caused by state-dependent linearizations. A suitable alternative is the IEKF, which relies on state-independent error dynamics. A detailed discussion on the limitations of linearization can be found in [34], where the IEKF, EKF, and ESEKF are compared for the alignment problem. The prerequisite for using the IEKF is the group affine property. Nevertheless, this condition is violated if IMU biases and drifts are explicitly modeled as states. Therefore the key challenge is to benefit from the IEKF framework while dealing with IMU uncertainties. In the proposed PI-IEKF, these uncertainties are

mitigated by reformulating the IEKF innovation into a PI structure. This approach builds on the following assumptions:

1. The navigation equations are considered in the Earth-Centered Inertial (ECI) frame.

2. The navigation states (attitude, velocity, position) are modeled on the Lie group SE2(3) (see Appendix A).

3. IMU measurements are affected by biases and drifts, but these are not explicitly included as states in order to preserve the group affine property.

5. GPS provides position observations, which are systematically expressed in a left-invariant form.

3. Theoretical Background of IEKF

A dynamical system is said to exhibit symmetry if some of its properties remain unchanged under a set of transformations. Invariant observers exploit such symmetries for estimation, and Lie groups provide the mathematical framework for their analysis [35]. In this paper, M is considered a Lie group, with m its corresponding Lie algebra. Basic definitions and notation are provided in Appendix A. The dynamics of a class of continuous stochastic systems whose state variables lie on M can be defined as Eq. (1) [23].

$$\frac{d}{dt}\chi_t = f_{u_t}(\chi_t) + \chi_t w_t \tag{1}$$

where $\chi_t \in \mathrm{M}$ is the state variable, u_t is the input, and $w_t \in m$ is Gaussian white noise. For this system, the left-invariant observation and the left-invariant error are defined as Eq. (2) and Eq. (3), respectively [23].

$$Y_t^L = \chi_t d_t + V_t \tag{2}$$

$$\eta_t^L = \chi_t^{-1}\hat{\chi}_t \tag{3}$$

where d is a known vector, V is Gaussian white noise, and $\hat{\chi}$ denotes the estimate of χ. If η_t^L follows a differential equation of the form $\frac{d}{dt}\eta_t^L = \Psi_{u_t}(\eta_t^L)$, it exhibits autonomous propagation, i.e., state-trajectory independence. Theorem 1, known as the group affine property (see Appendix B), enables the description of systems with autonomous errors without explicitly computing derivatives [23]. In this paper, GNSS measurements are employed, which can be expressed in left-invariant form. Therefore, the left-invariant extended Kalman filter (LIEKF) is adopted. For this purpose, the linearized discrete-time model of the left-invariant error is given as Eq. (4) [23, 36].

$$\xi_{k+1} = A_k\xi_k + G_k w_k \tag{4}$$

where ξ is the error state vector, A is the Jacobian of the dynamics model, nJacobiais the G of the dynamics process noise, and $w \sim \mathrm{N}(0, Q)$ is the process noise vector. The measurement error related to the left–invariant error states is calculated based on Eq. (5), given the measurement Y^L.

$$\delta y_k = \hat{\chi}_k^{-1}Y_k^L - d_k \tag{5}$$

where δy is the left-invariant error measurement. The linearized model of Eq. (5) is as Eq. (6).

$$\delta y_k = H_k\xi_k + \hat{\chi}^{-1}V_k \tag{6}$$

where H is the Jacobian of the invariant error measurement and $V \sim \mathrm{N}(0, R)$ is the measurement noise vector. H is used to calculate the Kalman gain and the covariance of the estimate. The propagation and update steps of the LIEKF are presented in **Algorithm 1** [23].

Algorithm 1: Left-Invariant Extended Kalman Filter (LIEKF)

1. Initialization $\hat{\chi}_0$ and P_0, and set $\hat{\xi}_0 = 0$.
2. **while** receiving data **do**
3. Calculation of the A_k and H_k matrices.
4. **if** Predict Step **then**
5. State Prediction: $\frac{d}{dt}\hat{\chi}_k^- = f_{u_t}(\hat{\chi}_{k-1})$ (7)
6. Error State Prediction: $\hat{\xi}_k^- = A_k\,\hat{\xi}_{k-1}$ (8)
7. Covariance Prediction: $P_k^- = A_k\,P_{k-1}\,A_k^T + Q_k$ (9)
8. **else if** Correction Step **then**
9. Innovation: $Z_k = \left(\hat{\chi}_k^-\right)^{-1} Y_k^L - d_k - H_k\hat{\xi}_k^-$ (10)
10. Kalman gain: $N_k = \left(\hat{\chi}_k^-\right)^{-1} R_k \left(\hat{\chi}_k^-\right)^{-T}$ $L_k = P_k^-\,H_k^T(H_k\,P_k^-\,H_k^T + N_k)^{-1}$ (11)
11. Error Stat Correction: $\hat{\xi}_k = \hat{\xi}_k^- + L_k Z_k$ (12)
12. Covariance Correction: $P_k = \left(I - L_k\,H_k\right)P_k^-\left(I - L_k\,H_k\right)^T + L_k\,N_k\,L_k^T$ (13)
13. Stat Correction: (Error Compensation) $\hat{\chi}_k = \hat{\chi}_k^-\exp\left(\left(\hat{\xi}_k\right)^\wedge\right)$ (14)
14. Error State Reset: $\hat{\xi}_k = 0$ (15)
15. **End**
16. Go to the next time step.
17. **End**

4. Proportional-Integral Invariant Extended Kalman Filter

The integral feedback loop is a well-established and effective technique in classical control systems. Its straightforward structure facilitates easy implementation and reduces computational load. Due to its robust performance, this approach has also been incorporated into estimation approaches, like the Kalman filter. The proportional-integral method has

effectively addressed the limitations of the Kalman filter related to the necessity for accurate system modeling, which is often impractical in practice [37]. Similar to the conventional Kalman filter, the proportional loop reduces the effects of process and measurement noise. At the same time, the integral loop enhances the system's robustness to modeling uncertainties and disturbances, which improves estimation accuracy in steady-state conditions [38, 39]. A brief history of PI estimator design is presented in [40]. The PI Kalman filter has been utilized for simultaneous state and fault estimation in time-varying linear systems with unknown inputs [41]. Additionally, it has been utilized to enhance robustness against convex uncertainties [38] and to improve the accuracy of INS/GPS integration [42]. Moreover, a proportional-integral-derivative (PID) filter inspired by PID controller principles has been proposed by [43]. This filter has been employed to perform the alignment of SINS in the presence of large misalignment angles [44], as well as for INS/GPS integration in the presence of measurement uncertainty [45]. There are two main approaches to incorporating the integral in KF [42]. The first approach integrates the integral state into the main system and computes the PI gains using the Kalman gain formula [43, 46, 47]. Although this method, similar to KF, achieves minimum error variance, it may be less successful in reducing the steady-state error. The second approach offers a more effective strategy for minimizing the steady-state error [42]. This method involves adding an integral state to the system, calculating the Kalman gain for the primary system, and deriving the PI gains for the augmented system. In this paper, the second approach is adopted, and the PI innovation term is defined as Eq. (16).

$$\begin{aligned} Z_{p_k} &= \left(\hat{\chi}_k^-\right)^{-1} Y_k^L - d_k - H_k \hat{\xi}_k^- \\ Z_{I_k} &= Z_{I_{k-1}} + k_{I_k} T_s Z_{p_k} \\ Z_{PI_k} &= k_{P_k} Z_{p_k} + Z_{I_{k-1}} \end{aligned} \tag{16}$$

where Z_{p_k} denotes the conventional innovation term, Z_{I_k} represents the integral innovation term, and Z_{PI_k} corresponds to the PI innovation term. The proportional and integral gains are

denoted by k_{P_k} and k_{I_k}, and T_s signifies the discretization time. By using the PI innovation in Eq. (16), the error state estimation relationship is modified as shown in Eq. (17).

$$\hat{\xi}_k = \hat{\xi}_k^- + L_k Z_{PI_k} \tag{17}$$

Additionally, Eq. (7) to Eq. (9) are employed in the prediction step, while Eq. (11), Eq. (13), and Eq. (14) are used in the update step. One of the requirements of this method is the determination of PI gains. This paper derives the PI gains by following the method proposed by [42], employing Lyapunov stability criteria and solving linear matrix inequalities. However, the relationships described in [42] are designed for a specific case and need to be generalized for use within the framework of this paper. Therefore, the augmented system is considered as Eq.(18).

$$x_k^{augment} = \left(\bar{A}_k - K_k \bar{B}_k\right) x_{k-1}^{augment} + u_k \tag{18}$$

where $x_k^{augment} = \begin{bmatrix} \xi_k \\ Z_{I_k} \end{bmatrix}$, $u_k = \begin{bmatrix} L_k k_{P_k} \\ k_{I_k} T_s \end{bmatrix} \delta y_k$, $K_{PI_k} = \begin{bmatrix} k_{P_k} \\ k_{I_k} \end{bmatrix}$, $\bar{A}_k = \begin{bmatrix} A_k & L_k \\ 0_{m\times n} & I_{m\times m} \end{bmatrix}$,

$\bar{B}_k = \begin{bmatrix} H_k A_k & 0_{m\times m} \end{bmatrix}$, $K_k = \begin{bmatrix} L_k & 0_{n\times m} \\ 0_{m\times m} & T_s I_{m\times m} \end{bmatrix} K_{PI_k}$ and n and m denote the number of states and measurements, respectively. One approach to calculate the gain matrix K_{PI_k} is to employ the Lyapunov stability criterion [42]. To this end, its discrete form for the system Eq. (18) is expressed by the following inequalities.

$$\left(\bar{A}_k - K_k \bar{B}_k\right)^T J_k \left(\bar{A}_k - K_k \bar{B}_k\right) - J_k < 0 \ , \ J_k = J_k^T > 0 \tag{19}$$

where J is a symmetric positive definite matrix. The inequality (19) guarantees system stability; however, it does not ensure any specific convergence rate of the states. The modification of the (19) as Eq. (20) guarantees convergence to zero at a rate higher than ρ.

$$\left(\bar{A}_k - K_k \bar{B}_k\right)^T J_k \left(\bar{A}_k - K_k \bar{B}_k\right) - J_k < -2\rho J_k \ , \ J_k = J_k^T > 0 \tag{20}$$

It should be noted that the first inequality in (20) is not an LMI because it contains the product of the variable matrices K and J. By employing the Schur complement lemma, Eq. (20) can be equivalently rewritten as Eq. (21).

$$\begin{bmatrix} -(1-2\rho) J_k & \bar{A}_k^T - \bar{B}_k^T K_k^T \\ \bar{A}_k - K_k \bar{B}_k & -J_k^{-1} \end{bmatrix} < 0 \ , \ J_K = J_K^T > 0 \tag{21}$$

Finally, as a result of pre- and post-multiplying the first inequality in Eq. (21) with $\begin{bmatrix} I_n & 0 \\ 0 & J_k \end{bmatrix}$ and defining $N_k = J_k K_k$, the following LMI is obtained.

$$\begin{bmatrix} -(1-2\rho) J_k & \bar{A}_k^T J_k - \bar{B}_k^T N_k^T \\ J_k \bar{A}_k - N_k \bar{B}_k & -J_k \end{bmatrix} < 0 \ , \ J_K = J_K^T > 0 \tag{22}$$

Finally, after solving the above LMIs and obtaining J_k and N_k, K_{PI_k} is calculated from the Eq.(23).

$$K_{PI_k} = \begin{bmatrix} L_k & 0_{n\times m} \\ 0_{m\times m} & T_s I_{m\times m} \end{bmatrix}^{-1} J_k^{-1} N_k \tag{23}$$

It is worth noting that an alternative LMI-based approach for gain derivation can be found in [48]. By combining the proposed algorithm with IEKF, IMU errors can be ignored, thereby satisfying the group affine property and enhancing accuracy. The proposed method is summarized in **Algorithm 2**. Its differences with IEKF are highlighted in the shaded form. It is worth noting that the proposed PI-IEKF still relies on the covariance optimization framework of the Kalman filter, while enhancing robustness through the PI innovation structure.

Algorithm 2: Proportional-Integral Left-Invariant Extended Kalman Filter (PI-LIEKF)

1. Initialization $\hat{\chi}_0$ and P_0, and set $\hat{\xi}_0 = 0$.
2. **while** receiving data **do**
3. Calculation of the A_k and H_k matrices.
4. **if** Predict Step **then**
5. State Prediction: $\frac{d}{dt}\hat{\chi}_k^- = f_{u_t}(\hat{\chi}_{k-1})$ (24)
6. Error State Prediction: $\hat{\xi}_k^- = A_k\,\hat{\xi}_{k-1}$ (25)
7. Covariance Prediction: $P_k^- = A_k\,P_{k-1}\,A_k^T + Q_k$ (26)
8. **else if** Correction Step **then**
9. Kalman gain: $N_k = \left(\hat{\chi}_k^-\right)^{-1} R_k \left(\hat{\chi}_k^-\right)^{-T}$, $L_k = P_k^-\,H_k^T (H_k\,P_k^-\,H_k^T + N_k)^{-1}$ (27)
10. Calculation of the PI gains using solving the LMI Eq. (22). (28)
11. Construction PI innovation: $Z_{PI_k} = k_{P_k} Z_{p_k} + Z_{I_{k-1}}$, $Z_{p_k} = \left(\hat{\chi}_k^-\right)^{-1} Y_k^L - d_k - H_k\hat{\xi}_k^-$, $Z_{I_k} = Z_{I_{k-1}} + k_{I_k} T_s Z_{p_k}$ (29)
12. Error Stat Correction: $\hat{\xi}_k = \hat{\xi}_k^- + L_k Z_{PI_k}$ (30)
13. Covariance Correction: $P_k = \left(I - L_k\,H_k\right)P_k^-\left(I - L_k\,H_k\right)^T + L_k\,N_k\,L_k^T$ (31)
14. Stat Correction: (Error Compensation) $\hat{\chi}_k = \hat{\chi}_k^- \exp\left(\left(\hat{\xi}_k\right)^\wedge\right)$ (32)
15. Error State Reset: $\hat{\xi}_k = 0$ (33)
16. **End**
17. Go to the next time step.
18. **End**

5. PI-IEKF Development for SINS Alignment in the ECI

In this section, the dynamic model of invariant error and invariant observations are introduced to perform SINS alignment in the ECI frame. In this paper, position measurements

obtained from GPS are used for the alignment process. Due to the left-invariance of GNSS observations [23], the dynamic model of the error and observations in the left-invariant form is presented. The Eq. (34) define the models for the gyroscope and accelerometer.

$$\begin{aligned}
\tilde{\omega}_{ib}^{b} &= \omega_{ib}^{b} + b^{g} + w^{g} \\
\tilde{f}_{ib}^{b} &= f_{ib}^{b} + b^{a} + w^{a} \\
\dot{b}^{g} &= w^{bg} \\
\dot{b}^{a} &= w^{ba}
\end{aligned} \tag{34}$$

where ω_{ib}^{b} and f_{ib}^{b} are the inputs, and $\tilde{\omega}_{ib}^{b}$ and $\tilde{f}_{ib}^{b}$ are the outputs of the IMU. b^{g} and b^{a} are the gyroscope drift and accelerometer bias vectors, respectively. w^{g}, w^{a}, w^{bg} and w^{ba} are the white noise vectors associated with the gyroscope and accelerometer.

5.1. Navigation Equations in ECI

The equations of attitude, velocity, and position in the ECI frame, with the ECI frame considered the inertial frame and the forward-left-up frame as the body frame, are given in Eq. (35).

$$\begin{aligned}
\dot{C}_{b}^{i}(t) &= C_{b}^{i}(t)\left(\tilde{\omega}_{ib}^{b}(t)\right)_{\times} \\
\dot{v}_{ib}^{i}(t) &= C_{b}^{i}(t)\,\tilde{f}_{ib}^{b}(t) + g(t) \\
\dot{p}_{ib}^{i}(t) &= v_{ib}^{i}(t)
\end{aligned} \tag{35}$$

where i and b represent the inertial and the body frame, respectively. C_{b}^{i} represents the attitude matrix that describes the orientation of b relative to i, and v_{ib}^{i} and p_{ib}^{i} are the velocity and the position vector of b relative to i, both expressed in the i. $(.)_{\times}$ represents the skew-symmetric matrix. $\tilde{\omega}_{ib}^{b}$ is the angular velocity and $\tilde{f}_{ib}^{b}$ is the acceleration of b with respect to i, both of which are measured by gyroscopes and accelerometers, respectively. g is the gravity vector.

5.2. Left-Invariant Error Model

INS variables can be considered as elements of the matrix Lie group $SE_2(3)$. In this case, the system state matrix is defined as Eq. (36) [23].

$$\chi_t = \begin{bmatrix} C_b^i(t) & v_{ib}^i(t) & p_{ib}^i(t) \\ 0_{1\times3} & 1 & 0 \\ 0_{1\times3} & 0 & 1 \end{bmatrix} \tag{36}$$

Ignoring the bias and drift errors of the IMU, the differential equation of the state matrix (36) could be written as Eq. (37), based on Eq. (34).

$$\frac{d}{dt}\chi_t = \frac{d}{dt}\begin{bmatrix} C_b^i(t) & v_{ib}^i(t) & p_{ib}^i(t) \\ 0_{1\times3} & 1 & 0 \\ 0_{1\times3} & 0 & 1 \end{bmatrix} = f_{u_t}(\chi_t) - \chi_t \left(w_t\right)^{\wedge} \tag{37}$$

where $w_t = \left[\left(w_t^g\right)^T, \left(w_t^a\right)^T, 0_{1\times3}\right]^T$ and $f_{u_t}(\chi_t) = \begin{bmatrix} C_b^i(t)\left(\omega_{ib}^b(t)\right)_{\times} & C_b^i(t)\left(f_{ib}^b(t)\right) + g(t) & v_b^i(t) \\ 0_{1\times3} & 0 & 0 \\ 0_{1\times3} & 0 & 0 \end{bmatrix}$.

To verify the group affine property $f_{u_t}(\chi_t)$ can be expressed as Eq. (38).

$$f_{u_t}(\chi_t) = \chi_t W_1 + W_2 \chi_t \tag{38}$$

where $W_1 = \begin{bmatrix} (\omega_{ib}^b(t))_{\times} & f_{ib}^b(t) & 0_{1\times3} \\ 0_{1\times3} & 0 & 1 \\ 0_{1\times3} & 0 & 0 \end{bmatrix}$ and $W_2 = \begin{bmatrix} 0_{3\times3} & g(t) & 0 \\ 0_{1\times3} & 1 & -1 \\ 0_{1\times3} & 0 & 0 \end{bmatrix}$. Using Eq. (38), for two arbitrary paths χ_A and χ_B from the states of the system (37), the relations $f_{u_t}(I_d) = W_1 + W_2$ and $f_{u_t}(\chi_A\chi_B) = \chi_A\chi_B\ W_1 + W_2\ \chi_A\chi_B$ are obtained. According to Theorem 1, the group affine property is checked as (39).

$$
\begin{aligned}
&f_{u_t}(\chi_A)\chi_B + \chi_A f_{u_t}(\chi_B) - \chi_A f_{u_t}(I_d)\chi_B = \\
&\chi_A W_1 \chi_B + W_2 \chi_A \chi_B + \chi_A \chi_B W_1 + \chi_A W_2 \chi_B - \chi_A (W_1 + W_2)\chi_B = \\
&\chi_A \chi_B W_1 + W_2 \chi_A \chi_B = f_{u_t}(\chi_A \chi_B)
\end{aligned}
\tag{39}
$$

It is clear that the group affine property holds, and therefore, the invariant error is state-independent. The left-invariant form of the error will be as Eq. (40).

$$
\eta_t^L = \chi_t^{-1}\hat{\chi}_t = \begin{bmatrix} C_i^b(t)\hat{C}_b^i(t) & C_i^b(t)\hat{v}_{ib}^i(t) - C_i^b(t)v_{ib}^i(t) & C_i^b(t)\hat{p}_{ib}^i(t) - C_i^b(t)p_{ib}^i(t) \\ 0_{1\times 3} & 1 & 0 \\ 0_{1\times 3} & 0 & 1 \end{bmatrix} \tag{40}
$$

where the symbol ^ represents the estimated values. The elements of the first row Eq. (40) represent the new error related to the attitude, velocity, and position, respectively. Unlike the conventional definition of error, which represents the direct difference between vectors in computational and real coordinates, new errors are defined within a common coordinate framework. This approach simultaneously takes into account the differences in both magnitude and direction between two vectors. Defining the error in this manner allows for a more accurate description of motion characteristics, leading to the verifiable convergence of the IEKF [49, 50]. Finally, considering ξ as the error state vector of the inertial navigation system in the Euclidean space corresponding to η^L, the matrices A and G, along with the vector w used in Eq. (8), are expressed as (41) [25].

$$
\begin{aligned}
&\zeta = \begin{bmatrix} \zeta^C \\ \zeta^v \\ \zeta^p \end{bmatrix},\ w = \begin{bmatrix} w^g \\ w^a \end{bmatrix},\ A = I_{9\times 9} + \begin{bmatrix} -\left(\tilde{\omega}_{ib}^b(t)\right)_\times & 0_{3\times 3} & 0_{3\times 3} \\ -(\tilde{f}_{ib}^b)_\times & -\left(\tilde{\omega}_{ib}^b(t)\right)_\times & 0_{3\times 3} \\ 0_{3\times 3} & I_{3\times 3} & -\left(\tilde{\omega}_{ib}^b(t)\right)_\times \end{bmatrix} T_s \\
&G = \begin{bmatrix} I_{3\times 3} & 0_{3\times 3} \\ 0_{3\times 3} & I_{3\times 3} \\ 0_{3\times 3} & 0_{3\times 3} \end{bmatrix} T_s
\end{aligned}
\tag{41}
$$

where ζ^C, ζ^v, and ζ^p are the vectors representing the attitude, velocity, and position errors, respectively. It is important to highlight that while the small angle approximation is applied to

derive the model (41), Theorem 2 (see Appendix B) confirms that the obtained model is exactly equivalent to the model derived without using this approximation [51].

5.3. Observation Model

The left-invariant form of the position measurement provided by GPS data is given by Eq. (42).

$$Y^L = \begin{bmatrix} p^i_{gps} \\ 0 \\ 1 \end{bmatrix} = \begin{bmatrix} C^i_b(t) & v^i_{ib}(t) & p^i_{ib}(t) \\ 0_{1\times 3} & 1 & 0 \\ 0_{1\times 3} & 0 & 1 \end{bmatrix} \begin{bmatrix} 0 \\ 0 \\ 1 \end{bmatrix} + \begin{bmatrix} w_{Gp} \\ 0 \\ 0 \end{bmatrix} \tag{42}$$

where p^i_{gps} is the position provided by GPS in the inertial frame, and w_{Gp} is the additive noise associated with the position measurement. In this case, the H matrix related to Eq. (6) is as Eq. (43).

$$H = \begin{bmatrix} 0_{3\times 3} & 0_{3\times 3} & I_{3\times 3} \end{bmatrix} \tag{43}$$

It can be seen from Eq. (41) and Eq. (43) that the matrices A and H are state-independent, which implies that the linearized models of the process and observation are not sensitive to the state estimation error. Figure 1 shows the block diagram of SINS alignment using the PI-IEKF.

6. Evaluation Through Simulation and Field Test Data

This section presents a simulation study aimed at evaluating the performance of the PI-IEKF in addressing the SINS alignment problem, using both synthetic and experimental data. The synthetic data was generated using MATLAB simulations for SINS alignment in a marine environment, while experimental data from the open-source KITTI dataset was employed for the alignment of a vehicle-mounted SINS system [52]. In a marine environment, a ship is subject to oscillatory motion caused by sea waves and other disturbances such as wind, which

can disrupt the output of inertial sensors and observations. Under these conditions, conventional alignment methods may not provide adequate effectiveness. In the first part, the performance of the PI-IEKF method in aligning a SINS system installed on a ship is evaluated using synthetic data. For data generation, an ideal path for the ship's movement in the ECI frame is assumed, which also serves as the reference for comparing results. Ideal data are generated by performing reverse navigation for this path. Following this, IMU measurements and GPS observations are obtained by adding noise to these ideal data. It is assumed that the inertial sensors are well-calibrated, and the gyroscope and accelerometer models are based on Eq. (34). The specifications of the sensor used in the simulations are presented in Table 1. The IMU output frequency is set to 100 Hz, and the GPS update rate is set to 1 Hz.

The roll, pitch, and yaw angles due to sea waves are considered as Eq. (44).

$$\begin{aligned} \phi &= 10^{\circ}\cos(\tfrac{2\pi}{6}t) \\ \theta &= 7^{\circ}\cos(\tfrac{2\pi}{5}t) \\ \psi &= 5^{\circ}\cos(\tfrac{2\pi}{7}t) \end{aligned} \tag{44}$$

here, φ, θ, and ψ refer to the roll, pitch, and yaw angles, respectively. The velocity variations are considered as Eq. (45).

$$\begin{aligned} &V_i = \frac{2\pi A_i}{T_i}\cos(\frac{2\pi}{T_i}t)\ ,\ i = x, y, z \\ &A_x = 10m/s\ ,\ A_y = 10m/s\ ,\ A_z = 1m/s\ ,\ T_x = 7s\ ,\ T_y = 6s\ ,\ T_z = 8s \end{aligned} \tag{45}$$

The initial assumptions for the process and measurement noise covariance matrices, as well as the initial guess, are provided in Table 2.

where $diag(.)$ and $blkdiag(.)$ represent the diagonal matrix and the block diagonal matrix, respectively. σ^2_{nAcc} and σ^2_{nGyro} denote the initial covariance of accelerometer and gyroscope noise, while σ^2_{φ}, σ^2_{θ}, and σ^2_{ψ} are the initial covariance of the Euler angle errors. A key

challenge in achieving alignment lies in accurately determining the yaw angle. Therefore, in the simulation, the initial errors of φ and θ angles are assumed to be constant at 10°. The error of ψ angle is varied within the range $[-90^{\circ} \quad 90^{\circ}]$ with a step of 30°. Figure 2 and Figure 3 show the estimation results of Euler angles and their corresponding errors using the PI-IEKF and imperfect IEKF methods for an initial yaw error of 60°, respectively. Additionally, the attitude estimation error for different initial yaw angle errors is shown in Figures 4 to 6.

The results indicate that both methods are effective in delivering accurate state estimation. In terms of convergence speed, the roll and pitch angles converge quickly and within a short time frame for both methods, with no significant differences observed between them. However, the yaw angle estimation converges faster using the PI-IEKF method. Furthermore, the yaw angle estimation by PI-IEKF demonstrates higher accuracy. The root mean square error (RMSE) of Euler angles estimations for the imperfect IEKF and PI-IEKF methods is presented in Table 3. As shown, the RMSE of the PI-IEKF estimation is lower than that of the imperfect IEKF. Additionally, considering that a large initial yaw angle error was assumed in this scenario, the results of both filters demonstrate their ability to handle large errors. This capability is one of the notable advantages of the IEKF, attributed to its use of a state-independent model.

The following section uses GPS and IMU data from the 2011_10_03_drive_0027 sequence, which is part of the KITTI dataset. This dataset was collected using sensors mounted on a vehicle, including a camera, GPS/IMU, and LiDAR. The data includes sensor outputs and ground truth information. The ground truth was calculated by combining the outputs of GPS/IMU and LiDAR. The OXTS RT 3003 GPS/IMU sensor, with its specifications presented in Table 4 [53], was used to measure GPS and IMU data.

The data were collected for 469 seconds while traversing the path shown in Figure 7. In this experiment, IMU outputs at a frequency of 100 Hz and GPS observations at a frequency of 1 Hz were utilized. The values used in the simulations are provided in Table 5.

According to the ground truth data, the true initial Euler angles are equal to $\varphi = 0.9067^{\circ}$, $\theta = 0.0463^{\circ}$ and $\psi = 61.6036^{\circ}$ respectively. The performance and efficiency of the PI-LIEKF method are analyzed under the assumption that the initial roll and pitch angles have a 10° error. Under these conditions, the performance of the PI-LIEKF is compared with that of the imperfect IEKF for initial yaw angle error values within the range of $[-90 \;\; 90]^{\circ}$. The estimation results of the Euler angles are illustrated in Figure 8, while Figures 9 to 11 present the corresponding estimation errors. As observed in these figures, the PI-LIEKF method outperforms the incomplete IEKF in both convergence speed and accuracy.

The evaluation results using experimental data confirm the superiority of the PI-LIEKF in achieving faster and more accurate yaw angle estimation compared to the imperfect IEKF. The results of this section confirm that the proposed PI-IEKF preserves the group-affine property, effectively compensates for IMU biases and drifts, remains robust to large initial misalignments, and provides faster convergence with improved accuracy compared to the IEKF.

7. Conclusions

This paper introduces a proportional-integral invariant Extended Kalman filter for SINS alignment. The IEKF addresses the limitations of the EKF caused by linearization by leveraging group theory and invariant theory. However, the group affine property of the system dynamics—a prerequisite for using the IEKF—is violated by IMU bias and drift. To overcome this limitation, which otherwise renders the IEKF unusable, the proposed method initially

disregards these errors. This restores the group affine property and enables the application of the IEKF. To manage uncertainties, the proportional innovation term of the KF is restructured into a PI form, which enhances the system's robustness and improves overall performance. The decision to employ the IEKF, enhanced with a PI innovation structure, rather than a fully nonlinear filter, is based on a fundamental balance between computational complexity, the specific structure of the problem, and the handling of IMU errors. The evaluation of the proposed method, using synthetic and experimental data, demonstrated significant advantages over the conventional IEKF, particularly regarding accuracy and convergence speed. These advantages are especially evident in the estimation of the yaw angle. As a result, the application of this method can significantly reduce the time required to initiate the navigation process. Finally, as a direction for future work, combining the IEKF with the H_∞ filter and smooth variable structure filters could be explored to further enhance the handling of uncertainties.

Statements and Declarations:

Competing Interests: The authors have no competing interests to declare that are relevant to the content of this article.

Acknowledgments: The authors have no acknowledgments to declare.

Data availability: The data used to support the findings of this study are available from the KITTI Vision Benchmark Suite at https://www.cvlibs.net/datasets/kitti/index.php.

Funding: The authors received no financial support for the research, authorship, and/or publication of this article.

Appendix A: Basic Definitions and Notation on Lie Groups

A Lie group combines the properties of a group and a smooth manifold. Each Lie group has an associated vector space called the Lie algebra. A matrix group refers to a set of square

matrices that satisfy the group axioms. Specifically, a matrix Lie group is a class of Lie groups that is simultaneously a matrix group [23]. The mapping from the vector space to m is done using the "hat" operator, $(\cdot)^{\wedge}$, and mapping from m to M is carried out via the exponential matrix, exp(·). The inverse mappings are performed using the "vee" operator, $(\cdot)^{\vee}$, and the logarithm matrix, log(·), respectively [54]. A widely-used Lie group in navigation and robotics is the group of double direct isometries, denoted as $SE_2(3)$. This group provides a framework for representing 3D orientation along with two additional vectors in $\mathbb{R}^3$, typically corresponding to velocity and position. $SE_2(3)$ is particularly advantageous for modeling motion-related variables, including attitude, velocity, and position. The definition of $SE_2(3)$ is as Eq. (A.1):

$$\mathrm{SE}_2(3)=\left\{\begin{bmatrix} \mathrm{C} & \mathrm{v} & \mathrm{p} \\ 0 & 1 & 0 \\ 0 & 0 & 1 \end{bmatrix} \in \mathbb{R}^{5\times5} \middle| \mathrm{C} \in \mathrm{SO}(3),\ \mathrm{v},\mathrm{p} \in \mathbb{R}^3 \right\} \tag{A.1}$$

where C represents the rotation matrix, v is the velocity vector and p is the position vector. The Lie algebra corresponding to $SE_2(3)$, denoted by $\mathrm{se}_2(3)$, is defined as Eq. (A.2) for $\xi \triangleq \mathrm{vec}(\phi, \vartheta, \mu) \in \mathbb{R}^9$.

$$\xi^{\wedge} \triangleq \begin{bmatrix} \phi_{\times} & \vartheta & \mu \\ 0_{1\times3} & 0 & 0 \\ 0_{1\times3} & 0 & 0 \end{bmatrix} \tag{A.2}$$

The exponential map from.)3A.(Eq. is also as $SE_2(3)$ to $\mathrm{se}_2(3)$

$$\exp(\xi^{\wedge})=\begin{bmatrix} \exp(\phi_{\times}) & \tau\vartheta & \tau\mu \\ 0_{1\times3} & 1 & 0 \\ 0_{1\times3} & 0 & 1 \end{bmatrix}, \qquad \tau = \mathrm{I} + \frac{1-\cos\|\phi\|}{\|\phi\|^2}\phi_{\times} + \frac{\|\phi\|-\sin\|\phi\|}{\|\phi\|^3}\phi_{\times}^2 \tag{A.3}$$

The logarithm map from.)4A.(Eq. is as $se_2(3)$ to $SE_2(3)$

$$\log(\xi)=\begin{bmatrix} \log(C) & \tau^{-1}\mu & \tau^{-1}\mu \\ 0_{1\times 3} & 0 & 0 \\ 0_{1\times 3} & 0 & 0 \end{bmatrix} \in \square^{9}, \quad \tau^{-1} = \mathrm{I} - \frac{1}{2}\phi_{\times} + \frac{1}{\|\phi\|^2}\left(1 - \frac{\|\phi\|\sin\|\phi\|}{2(1-\cos\|\phi\|)}\right)\phi_{\times}^2 \qquad (A.4)$$

Appendix B: Key Theorems

Theorem 1 - Group Affine property[23]: System (1) has a state-trajectory-independent left or right-invariant error if the following condition holds.

$$f_{u_t}(ab) = f_{u_t}(a)b + a\, f_{u_t}(b) - a\, f_{u_t}(I_d)b \quad for\ all\ a,b \in \mathrm{M}\ ,\ t>0 \qquad (B.1)$$

where I_d is the group identity element. Systems in the form Eq. (1) that possess independent invariant errors exhibit remarkable properties that generalize linear systems. One of these features is the log-linear property of the error propagation (Theorem 2 [23]).

Theorem 2- Linearity of the logarithm of the error: If, for the invariant error η_t, $\xi_0 \in \square^{n}$ satisfies $\exp\left((\xi_0)^{\wedge}\right) = \eta_0$ and the F_t matrix establishes the $\Psi_{u_t}\left(\exp(\xi^{\wedge})\right) = (F_t\xi)^{\wedge} + O(\|\xi\|^2)$, then, if the linear differential equation $\frac{d}{dt}\xi_t = F_t\xi_t$ holds for $t>0$, then the nonlinear error η_t for $t \geq 0$ follows the $\eta_t = \exp((\xi_t)^{\wedge})$.

The above theorem demonstrates that despite the approximation,can be accurately η_t recovered from the linear differential equation related to ξ_t. In fact, with the appropriate choice of the error variable, many nonlinear problems can be transformed into linear error equations.

REFERENCES

[1] Titterton, D. H. and Weston, J. L., "Strapdown inertial navigation technology", *Institution of Engineering and Technology (IET)*, (2004). https://doi.org/10.1049/PBRA017E

[2] Noureldin, A., Karamat, T. B., and Georgy, J., "Fundamentals of inertial navigation, satellite-based positioning and their integration", *Springer Science and Business Media*, (2013). https://doi.org/10.1007/978-3-642-30466-8

[3] Rogers, R. M., "Applied mathematics in integrated navigation systems", *American Institute of Aeronautics and Astronautics (AIAA)*, (2007). https://doi.org/10.1017/S0001924000087947

[4] Chang, L., Qin, F., and Jiang, S., "Strapdown inertial navigation system initial alignment based on modified process model", *IEEE Sensors Journal*, 19(15), pp. 6381–6391 (2019). https://doi.org/10.1109/JSEN.2019.2910213

[5] Wang, K., Gao, W., Xu, X., and Wang, J., "Adaptive alignment for low-cost INS in ECEF frame under large initial attitude errors", *NAVIGATION: Journal of the Institute of Navigation*, 70(1), (2023). https://doi.org/10.33012/navi.554

[6] Ghanbarpourasl, H., "A new robust quaternion-based initial alignment algorithm for stationary strapdown inertial navigation systems", *Proceedings of the Institution of Mechanical Engineers, Part G: Journal of Aerospace Engineering*, 234(12), pp. 1913–1925 (2020). https://doi.org/10.1177/0954410020920473

[7] Rahimi, H., Nikkhah, A. A., and Hooshmandi, K., "A fast alignment of marine strapdown inertial navigation system based on adaptive unscented Kalman filter", *Transactions of the Institute of Measurement and Control*, 43(4), pp. 749–758 (2021). https://doi.org/10.1177/0142331220934

[8] Guo, S. L., Sun, Y. J., Chang, L. M., and Li, Y., "Robust cubature Kalman filter method for the nonlinear alignment of SINS", *Defence Technology*, 17(2), pp. 593–598 (2021). https://doi.org/10.1016/j.dt.2020.03.016

[9] Lin, Y., Miao, L., and Zhou, Z., *et al.*, "An improved MCMC-based particle filter for GPS-aided SINS in-motion initial alignment", *IEEE Transactions on Instrumentation and Measurement*, 69(10), pp. 7895–7905 (2020). https://doi.org/10.1109/TIM.2020.2986610

[10] Zhu, B., Li, D., Li, Z., He, H., and Li, X., "Robust adaptive Kalman filter for strapdown inertial navigation system dynamic alignment", *IET Radar, Sonar & Navigation*, 15(12), pp. 1583–1593 (2021). https://doi.org/10.1049/rsn2.12148

[11] Wu, M., Wu, Y., Hu, X., and Hu, D., "Optimization-based alignment for inertial navigation systems: Theory and algorithm", *Aerospace Science and Technology*, 15(1), pp. 1–17 (2011). https://doi.org/10.1016/j.ast.2010.05.004

[12] Huang, Y., Zhang, Y., and Chang, L., "A new fast in-motion coarse alignment method for GPS-aided low-cost SINS", *IEEE/ASME Transactions on Mechatronics*, 23(3), pp. 1303–1313 (2018). https://doi.org/10.1109/TMECH.2018.2835486

[13] Jameian, H., Safarinejadian, B., and Shasadeghi, M., "A robust and fast self-alignment method for strapdown inertial navigation system in rough sea conditions", *Ocean Engineering*, 187, p. 106196 (2019). https://doi.org/10.1016/j.oceaneng.2019.106196

[14] Ouyang, W. and Wu, Y., "Optimization-based strapdown attitude alignment for high-accuracy systems: Covariance analysis with applications", *IEEE Transactions on Aerospace and Electronic Systems*, 58(5), pp. 4053–4069 (2022). https://doi.org/10.1109/TAES.2022.3157570

[15] Liu, W., Duan, R., and Zhu, F., "A robust cascaded strategy of in-motion alignment for inertial navigation systems", *International Journal of Distributed Sensor Networks*, 13(9), p. 1550147717732919 (2017). https://doi.org/10.1177/1550147717732919

[16] Thrun, S., Burgard, W., and Fox, D., "Probabilistic robotics", *The MIT Press*, (2005). https://doi.org/10.1017/S0269888906210993

[17] Simon, D., "Optimal state estimation: Kalman, H-infinity, and nonlinear approaches", *John Wiley and Sons*, (2006). https://doi.org/10.1002/0470045345

[18] Song, Y. and Grizzle, J. W., "The extended Kalman filter as a local asymptotic observer for nonlinear discrete-time systems", *Journal of Mathematical Systems Estimation and Control*, 5(1), pp. 59–78 (1995). https://doi.org/10.23919/ACC.1992.4792775

[19] Krener, A. J., "The convergence of the extended Kalman filter", *in Directions in Mathematical Systems Theory and Optimization*, Springer, Berlin, Heidelberg, pp. 173–182 (2003). https://doi.org/10.1007/3-540-36106-5_12

[20] Huang, G. P., Mourikis, A. I., and Roumeliotis, S. I., "Observability-based rules for designing consistent EKF SLAM estimators", *The International Journal of Robotics Research*, 29(5), pp. 502–528 (2010). https://doi.org/10.1177/0278364909353640

[21] Huang, G. P., Mourikis, A. I., and Roumeliotis, S. I., "A quadratic-complexity observability-constrained unscented Kalman filter for SLAM", *IEEE Transactions on Robotics*, 29(5), pp. 1226–1243 (2013). https://doi.org/10.1109/TRO.2013.2267991

[22] Barczyk, M. and Lynch, A. F., "Invariant observer design for a helicopter UAV aided inertial navigation system", *IEEE Transactions on Control Systems Technology*, 21(3), pp. 791–806 (2012). https://doi.org/10.1109/TCST.2012.2195495

[23] Barrau, A. and Bonnabel, S., "The invariant extended Kalman filter as a stable observer", *IEEE Transactions on Automatic Control*, 62(4), pp. 1797–1812 (2017). https://doi.org/10.1109/TAC.2016.2594085

[24] Potokar, E. R., Norman, K., and Mangelson, J. G., "Invariant extended Kalman filtering for underwater navigation", *IEEE Robotics and Automation Letters*, 6(3), pp. 5792–5799 (2021). https://doi.org/10.1109/LRA.2021.3085167

[25] Tang, J., Bian, H., Ma, H., and Wang, R., "SINS/GNSS integrated navigation based on invariant error models in inertial frame", *IEEE Sensors Journal*, 24(4), pp. 4290-4303 (2024). https://doi.org/10.1109/JSEN.2023.3346873

[26] Fu, H., Cheng, Y., and Zhang, T., "A new invariant extended Kalman filter based initial alignment method of SINS under large misalignment angle", *Proceedings of the 2021 China Automation Congress (CAC)*, pp. 57–62 (2021). https://doi.org/10.1109/CAC53003.2021.9728059

[27] Chang, L., Qin, F., and Xu, J., "Strapdown inertial navigation system initial alignment based on group of double direct spatial isometries", *IEEE Sensors Journal*, 22(1), pp. 803–818 (2021). https://doi.org/10.1109/JSEN.2021.3108497

[28] Li, D., Guo, W., Lou, Q., Liu, C., Luo, H., and Yu, X., "A rapid alignment method for high-precision rotational INS within group affine", *Measurement Science and Technology*, 35(7), p. 075106 (2024). https://doi.org/10.1088/1361-6501/ad3d77

[29] Liu, C., *et al.*, "A group affine-based inverse alignment method for high-precision rotational inertial navigation systems", *Sensors*, 25(6), p. 1767 (2025). https://doi.org/10.3390/s25061767

[30] Sheng, G., *et al.*, "A marine SINS transfer alignment method based on group affine of nonlinear state error in local-level frame", *Ocean Engineering*, 302, p. 117569 (2024). https://doi.org/10.1016/j.oceaneng.2024.117569

[31] Chang, L., Bian, Q., Zuo, Y., and Zhou, Q., "SINS/GNSS-integrated navigation based on group affine SINS mechanization in local-level frame", *IEEE/ASME Transactions on Mechatronics*, 28(5), pp. 2471–2482 (2023). https://doi.org/10.1109/TMECH.2023.3252044

[32] Zhang, Z., Zhao, J., Huang, C., and Li, L., "Precise and robust sideslip angle estimation based on INS/GNSS integration using invariant extended Kalman filter", *Proceedings of the Institution of Mechanical Engineers, Part D: Journal of Automobile Engineering*, (2022). https://doi.org/10.1177/09544070221102662

[33] Barrau, A. and Bonnabel, S., "The geometry of navigation problems", *IEEE Transactions on Automatic Control*, 68(2), pp. 689–704 (2022). https://doi.org/10.1109/TAC.2022.3144328

[34] Rajabi, M. J., Dehghan, S. M. M., and Mohammad-Hosseini, S., "Using invariant extended Kalman filter to integrate inertial navigation system and global positioning system", *Journal of Control*, 18(2), pp. 37–53 (2024).

[35] Bonnabel, S., Martin, P., and Rouchon, P., "Symmetry-preserving observers", *IEEE Transactions on Automatic Control*, 53(11), pp. 2514–2526 (2008). https://doi.org/10.1109/TAC.2008.2006929

[36] Barrau, A. and Bonnabel, S., "Invariant Kalman filtering", *Annual Review of Control, Robotics, and Autonomous Systems*, 1, pp. 237–257 (2018). https://doi.org/10.1146/annurev-control-060117-105010

[37] Kim, K., Shafai, B., and Kappos, E., "Proportional integral estimator", *Proceedings of the Signal and Data Processing of Small Targets 1989*, 1096, pp. 187–208 (1989). https://doi.org/10.1117/12.960353

[38] Jung, J., Han, S., and Huh, K., "Robust proportional-integral Kalman filter design using a convex optimization method", *Journal of Mechanical Science and Technology*, 22(5), pp. 879–886 (2008). https://doi.org/10.1007/s12206-007-1118-2

[39] Shafai, B. and Saif, M., "Proportional-integral observer in robust control, fault detection, and decentralized control of dynamic systems", *in Control and Systems Engineering: A Report on Four Decades of Contributions*, El-Osery, A. and Prevost, J. (Eds.), Springer International Publishing, Cham, pp. 13–43 (2015). https://doi.org/10.1007/978-3-319-14636-2_2

[40] Bakhshande, F. and Söffker, D., "Proportional-integral-observer: A brief survey with special attention to the actual methods using ACC benchmark", *IFAC-PapersOnLine*, 48(1), pp. 532–537 (2015). https://doi.org/10.1016/j.ifacol.2015.05.049

[41] Khemiri, K., Gannouni, F., Ben Hmida, F., Gossa, M., and Ragot, J., "Robust fault and state estimation for linear discrete-time systems with unknown disturbances using PI three-stage Kalman filter", *Proceedings of the International Conference on Communications, Computing and Control Applications (CCCA)*, Hammamet, Tunisia, pp. 1-7 (2011). https://doi.org/10.1109/CCCA.2011.6031199

[42] Shaghaghian, A. and Karimaghaee, P., "Improving GPS/INS integration using FIKF-filtered innovation Kalman filter", *Asian Journal of Control*, 21(4), pp. 1671–1680 (2019). https://doi.org/10.1002/asjc.1931

[43] Zhang, J., He, X., and Zhou, D., "Generalised proportional–integral–derivative filter", *IET Control Theory & Applications*, 10(17), pp. 2339–2347 (2016). https://doi.org/10.1049/iet-cta.2015.0610

[44] Rahgoshay, M. A., Karimaghaee, P., and Shabaninia, F., "Initial alignment of fiber-optic inertial navigation system with large misalignment angles based on generalized proportional-integral-derivative filter", *International Journal on Smart Sensing and Intelligent Systems*, 10(3), pp. 1–17 (2017). https://doi.org/10.21307/ijssis-2017-226

[45] Ansari, M., Jamali, J., Fatehi-Dindarlou, M. H., Rahgoshay, M. A., and Mahdiyar, O., "A novel sensor integration scheme for an aided inertial navigation system based on a generalized PID filter in the presence of observation uncertainty", *International Journal of Engineering*, 37(6), pp. 1127–1135 (2024). https://doi.org/10.5829/ije.2024.37.06c.09

[46] Linder, S. P. and Shafai, B., "Robust PFI Kalman filters", *Proceedings of the 1998 American Control Conference (ACC)*, vol. 5, pp. 3163–3164 (1998). https://doi.org/10.1109/ACC.1998.688445

[47] Bas, O. Y., Shafai, B., and Linder, S. P., "Design of optimal gains for the proportional integral Kalman filter with application to single particle tracking", *Proceedings of the 38th IEEE Conference on Decision and Control (CDC)*, vol. 5, pp. 4567–4571 (1999). https://doi.org/10.1109/CDC.1999.833262

[48] Hosseini-Pishrobat, M. and Keighobadi, J., "Robust vibration control and angular velocity estimation of a single-axis MEMS gyroscope using perturbation compensation", *Journal of Intelligent & Robotic Systems*, 94(1), pp. 61–79 (2019). https://doi.org/10.1007/s10846-018-0789-5

[49] Andrle, M. S. and Crassidis, J. L., "Attitude estimation employing common frame error representations", *Journal of Guidance, Control, and Dynamics*, 38(9), pp. 1614–1624 (2015). https://doi.org/10.2514/1.G001025

[50] Cui, J., Wang, M., Wu, W., and He, X., "Lie group-based nonlinear state errors for MEMS-IMU/GNSS/magnetometer integrated navigation", *The Journal of Navigation*, 74(4), pp. 887–900 (2021). https://doi.org/10.1017/S037346332100014X

[51] Chang, L. and Luo, Y., "Log-linear error state model derivation without approximation for INS", *IEEE Transactions on Aerospace and Electronic Systems*, 59(2), pp. 2029–2035 (2022). https://doi.org/10.1109/TAES.2022.3197726

[52] Geiger, A., Lenz, P., Stiller, C., and Urtasun, R., "Vision meets robotics: The KITTI dataset", *The International Journal of Robotics Research*, 32(11), pp. 1231–1237 (2013). https://doi.org/10.1177/0278364913491297

[53] OxTS, "RTv2 GNSS-aided inertial measurement systems user manual", [Online]. Available: www.oxts.com/app/uploads/2018/02/rtman.pdf (2018).

[54] Barfoot, T. D., "State estimation for robotics", *Cambridge University Press*, (2024). https://doi.org/10.1017/9781009299909

List of Captions

Figures

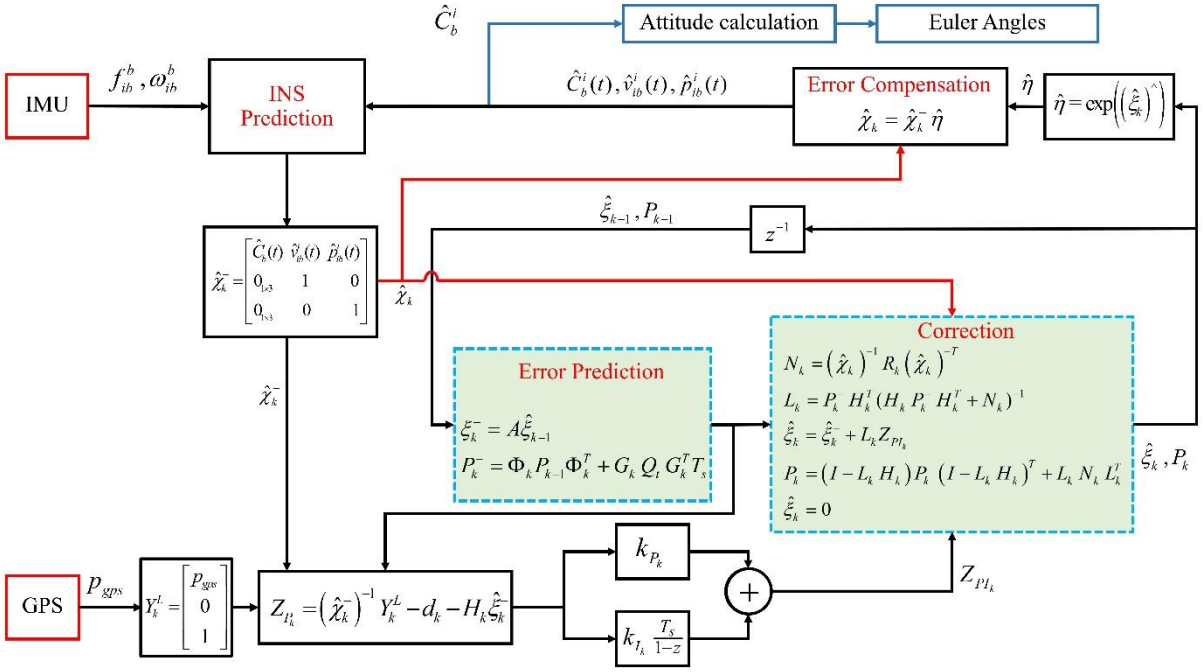

Figure 1. The block diagram of the proposed PI-LIEKF for SINS alignment

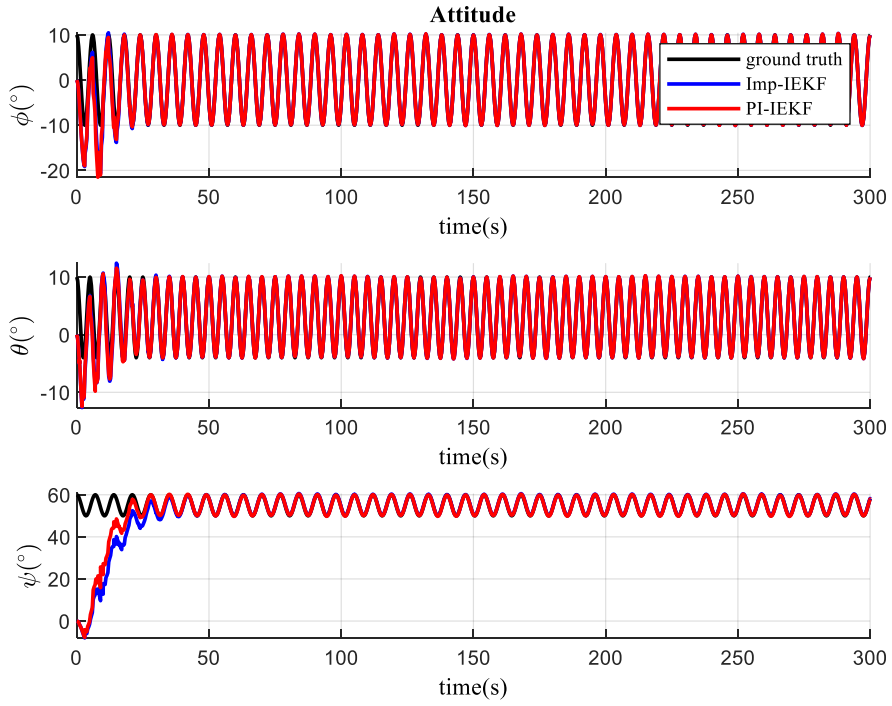

Figure 2. Estimation of Euler angles for an initial misalignment of 10° in roll and pitch and 60° in yaw

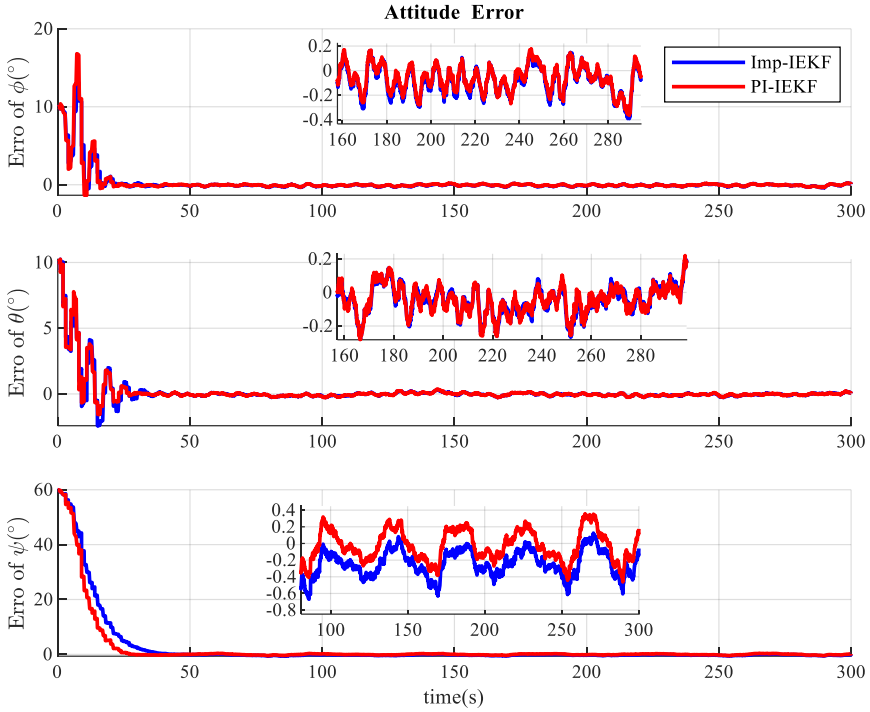

Figure 3. Euler angle estimation error for an initial misalignment of 10° in roll and pitch and 60° in yaw

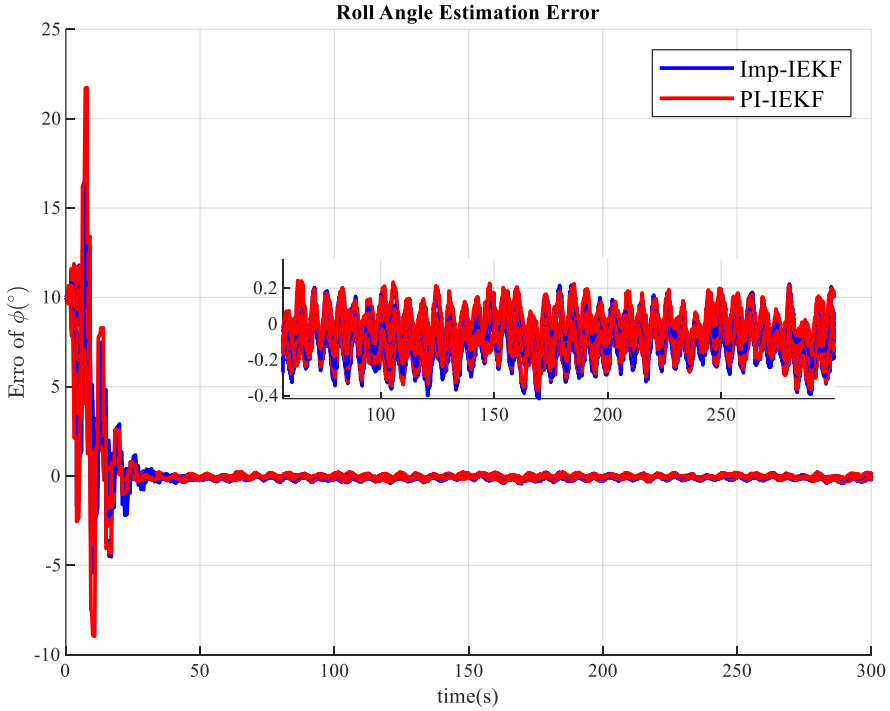

Figure 4. Roll angle estimation error for a 10° initial misalignment in roll and pitch with various initial yaw misalignments

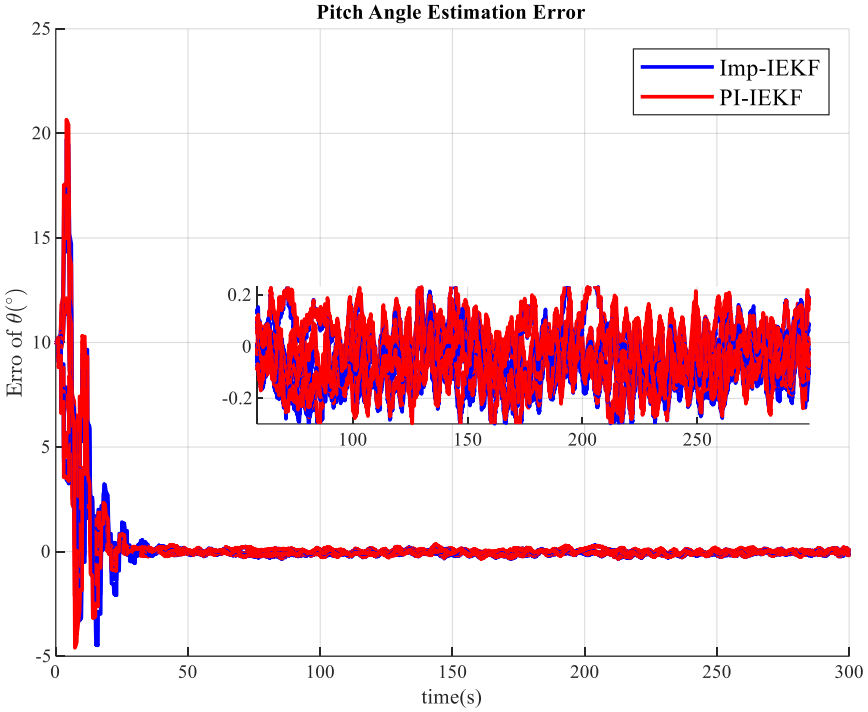

Figure 5. Pitch angle estimation error for a 10° initial misalignment in roll and pitch with various initial yaw misalignments

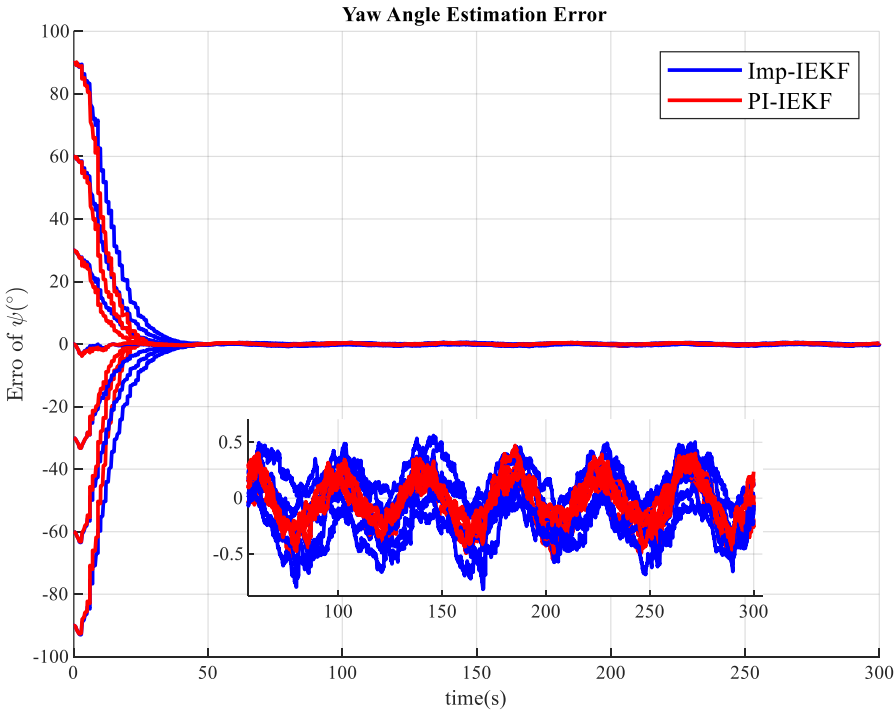

Figure 6. Yaw angle estimation error for a 10° initial misalignment in roll and pitch with various initial yaw misalignments

Figure 7. Trajectory of 2011_10_03_drive_0027 Sequence

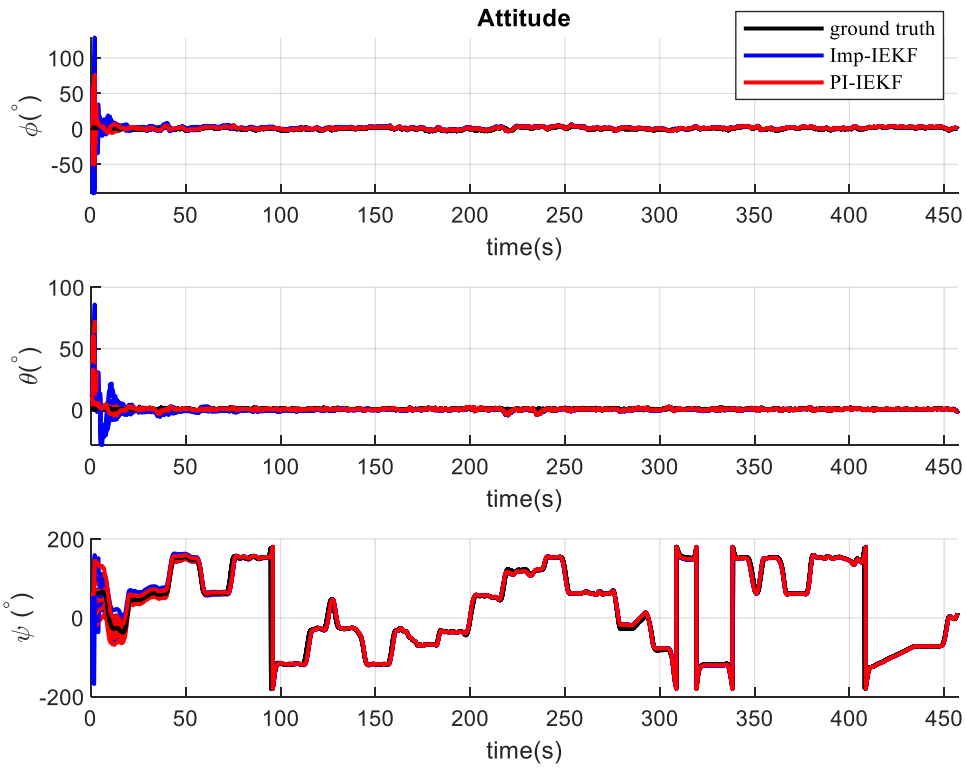

Figure 8. Estimation of Euler angles under different initial errors using experimental data

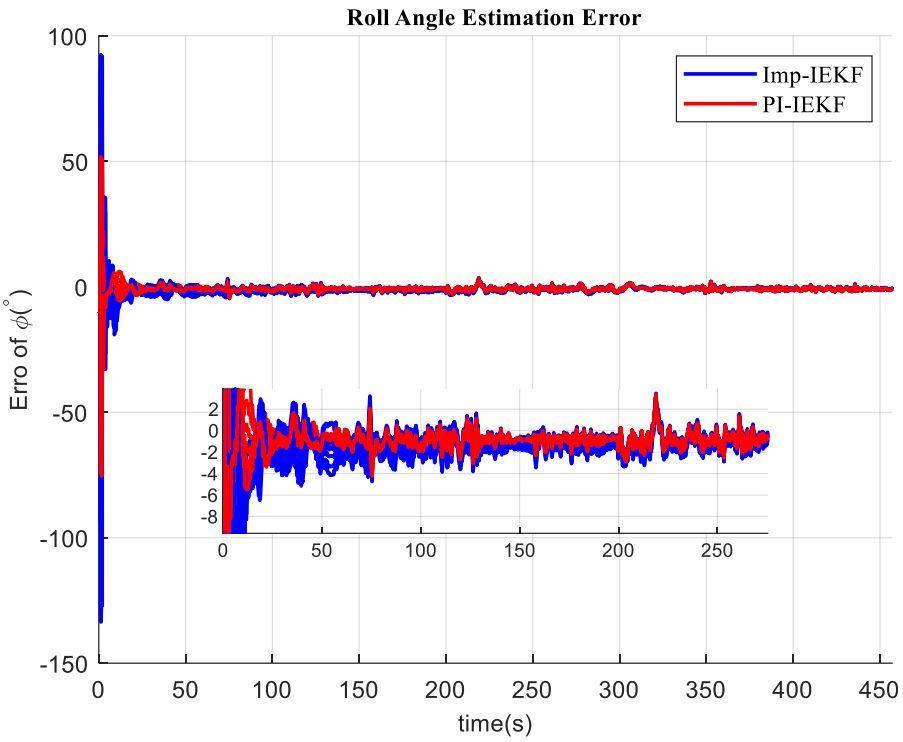

Figure 9. Estimation error of roll angle under different initial errors using experimental data

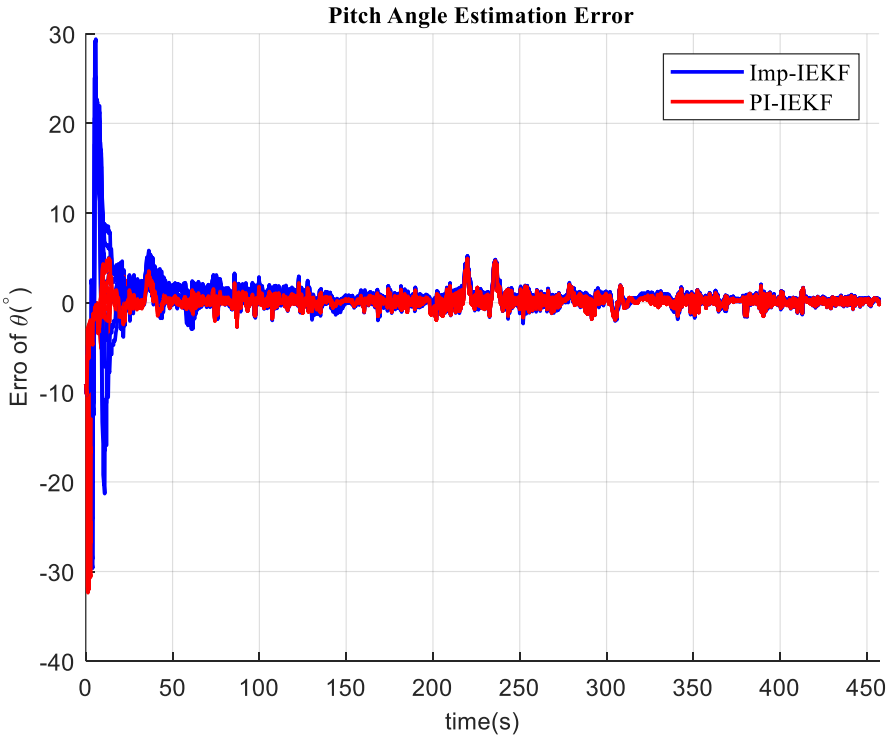

Figure 10. Estimation error of pitch angle under different initial errors using experimental data

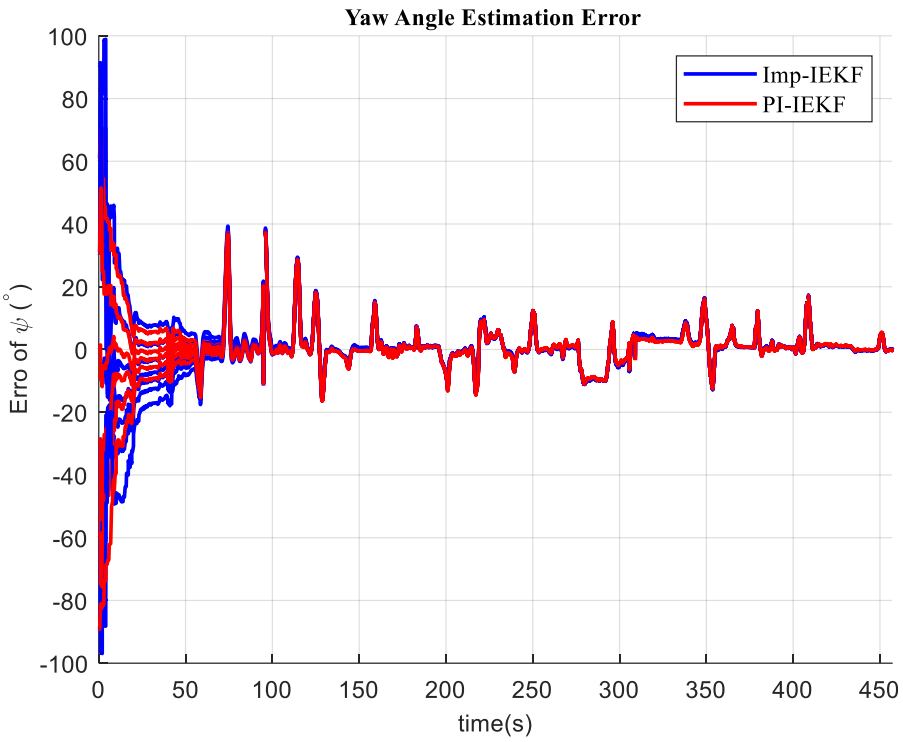

Figure 11. Estimation error of yaw angle under different initial errors using experimental data

Tables

Table 1. Specifications of IMU and GPS Used for Generating Synthetic Data

Sensor		Index	Symbol	Unit	Value
IMU	Gyroscopes	Bias Stability	b_{Gyro}	$^\circ/_{hr}$	25.2
		Angular Random Walk	ARW	$^\circ/\sqrt{hr}$	2.0
	Accelerometer	Bias Stability	b_{Acc}	mg	0.2
		Velocity Random Walk	VRW	$m/s\sqrt{hr}$	0.2
GPS		Velocity Accuracy	σ_{vGPS}	m/s	0.1
		Position Accuracy	σ_{pGPS}	m	1.0

Table 2. Values used in synthetic data simulations

Parameter	Filter	
	IEKF	PI-IEKF
R	$blkdiag\left(\sigma_{pGPS}^2 \times I_{3\times3}\right)$	$blkdiag\left(\sigma_{pGPS}^2 \times I_{3\times3}\right)$
Q	$diag\left(\sigma_{nGyro}^2 \times I_{3\times3}, \sigma_{nAcc}^2 \times I_{3\times3}, 0_{9\times9}\right)$	$diag\left(\sigma_{nGyro}^2 \times I_{3\times3}, \sigma_{nAcc}^2 \times I_{3\times3}, 0_{3\times3}\right)$
$[\varphi_0, \theta_0, \psi_0]$	$[0,0,0]^\circ$	$[0,0,0]^\circ$
x_0	$[0,0,0]m$	$[0,0,0]m$
v_0	$[0,0,0]\frac{m}{s}$	$[0,0,0]\frac{m}{s}$
P_0	$blkdiag\begin{pmatrix} diag[\sigma_\varphi^2, \sigma_\theta^2, \sigma_\psi^2], \dots \\ \sigma_{vGPS}^2 \times I_{3\times3}, \sigma_{pGPS}^2 \times I_{3\times3}, \dots \\ b_{Gyro}^2 \times I_{3\times3}, b_{Acc}^2 \times I_{3\times3} \end{pmatrix}$	$blkdiag\begin{pmatrix} diag[\sigma_\varphi^2, \sigma_\theta^2, \sigma_\psi^2], \dots \\ \sigma_{vGPS}^2 \times I_{3\times3}, \sigma_{pGPS}^2 \times I_{3\times3} \end{pmatrix}$
ρ	—	0.01

Table 3. RMSE of Euler angles for a 10° initial misalignment in roll and pitch and a 60° in yaw

RMSE	Imperfect IEKF	PI-IEKF
φ(deg)	1.59	1.61
θ(deg)	1.20	1.24
ψ(deg)	4.8	4.4

Table 4. Specifications of IMU and GPS sensors used in OXTS RT3003 [53]

Sensor		Index	Symbol	Unit	Value
IMU	Gyroscopes	Bias Stability	b_{Gyro}	$^{\circ}/_{hr}$	2
		Random Walk	ARW	$^{\circ}/\sqrt{hr}$	0.2
	Accelerometer	Bias Stability	b_{Acc}	μg	2
		Random Walk	VRW	$^{m}/_{s\sqrt{hr}}$	0.005
GPS		Velocity Accuracy	σ_{vGPS}	$^{km}/_{hr}$	0.05
		Position Accuracy	σ_{pGPS}	m	0.01

Table 5. Values used in the simulation of experimental data

Parameter	Filter	
	IEKF	PI-IEKF
R	$blkdiag\left(\sigma_{pGPS}^2 \times I_{3\times3}\right)$	$blkdiag\left(\sigma_{pGPS}^2 \times I_{3\times3}\right)$
Q	$diag\left(\sigma_{nGyro}^2 \times I_{3\times3}, \sigma_{nAcc}^2 \times I_{3\times3}, 0_{9\times9}\right)$	$diag\left(\sigma_{nGyro}^2 \times I_{3\times3}, \sigma_{nAcc}^2 \times I_{3\times3}, 0_{3\times3}\right)$
$[\varphi_0, \theta_0, \psi_0]$	$[0.9067, 0.0463, 61.6036]^{\circ}$	$[0.9067, 0.0463, 61.6036]^{\circ}$
x_0	$[1.0811, 1.3375, 0.7956]m$	$[1.0811, 1.3375, 0.7956]m$
v_0	$[0,0,0]\,^{m}/_{s}$	$[0,0,0]\,^{m}/_{s}$
P_0	$blkdiag\begin{pmatrix} diag[\sigma_{\varphi}^2, \sigma_{\theta}^2, \sigma_{\psi}^2], \dots \\ \sigma_{vGPS}^2 \times I_{3\times3}, \sigma_{pGPS}^2 \times I_{3\times3}, \dots \\ b_{Gyro}^2 \times I_{3\times3}, b_{Acc}^2 \times I_{3\times3} \end{pmatrix}$	$blkdiag\begin{pmatrix} diag[\sigma_{\varphi}^2, \sigma_{\theta}^2, \sigma_{\psi}^2], \dots \\ \sigma_{vGPS}^2 \times I_{3\times3}, \sigma_{pGPS}^2 \times I_{3\times3} \end{pmatrix}$
ρ	—	0.01

Biographies

Mohammad Javad Rajabi received the B.Sc. degree in Robotic Engineering from Hamedan University of Technology, Hamedan, Iran, in 2015, and the M.Sc. degree in Control Engineering from Malek-Ashtar University of Technology, Tehran, Iran, in 2017. He is currently pursuing the Ph.D. degree in Control Engineering with the Department of Control and Robotics, Malek-Ashtar University of Technology, Tehran, Iran. His research interests include nonlinear control, estimation, and navigation.

S.M. M. Dehghan received the B.Sc. degree in Electrical and Computer Engineering, the M.Sc. degree in Artificial Intelligence and Robotics, and the Ph.D. degree in Control Engineering from the University of Tehran, Tehran, Iran, in 1999, 2002, and 2015, respectively. His current research interests include autonomous aerospace systems, aerial robotics, navigation, complex and multi-agent systems, UAV cooperation, SLAM, and attitude determination and control. He is currently an Associate Professor with the Department of Control and Robotics, Malek-Ashtar University of Technology, Tehran, Iran.

S. Mohammad-Hosseini received the B.Sc. degree in Electrical Engineering from Ferdowsi University of Mashhad, Mashhad, Iran, in 1998, and the M.Sc. and Ph.D. degrees in Electrical Engineering from Iran University of Science and Technology, Tehran, Iran, in 2000 and 2009, respectively. His research interests include adaptive neural network control and nonlinear control. He is currently an Associate Professor with the Faculty of Electroceram Engineering, Malek-Ashtar University of Technology, Tehran, Iran.